Journal of Molecular Catalysis A: Chemical 427 (2017) 54–61

Contents lists available at ScienceDirect

Journal of Molecular Catalysis A: Chemical

journal homepage: www.elsevier.com/locate/molcata

Enhanced photocatalytic activity of Zn/Ti-LDH via hybridizing with C60

Yanping Zhu[a,b], Minwang Laipan[a,b], Runliang Zhu[a,*], Tianyuan Xu[a,b], Jing Liu[a,b], Jianxi Zhu[a,*], Yunfei Xi[c,d], Gangqiang Zhu[e], Hongping He[a]

[a] CAS Key Laboratory of Mineralogy and Metallogeny/Guangdong Provincial Key Laboratory of Mineral Physics and Materials, Guangzhou Institute of Geochemistry, Chinese Academy of Sciences(CAS), Guangzhou 510640, China
[b] University of Chinese Academy of Sciences, Beijing 100049, China
[c] School of Chemistry, Physics and Mechanical Engineering, Queensland University of Technology (QUT), GPO Box 2434, Brisbane, Queensland 4001, Australia
[d] Institute of Future Environments, Queensland University of Technology (QUT), GPO Box 2434, Brisbane, Queensland 4001, Australia
[e] School of Physics and Information Technology, Shaanxi Normal University, Xi'an, 710062, China

ARTICLE INFO

Article history:
Received 29 July 2016
Received in revised form 28 October 2016
Accepted 22 November 2016
Available online 23 November 2016

Keywords:
C60
Layered double hydroxides
Photocatalysis
Hybridization
Wastewater treatment

ABSTRACT

A novel and efficient photocatalyst was synthesized by surface hybridizing Zn/Ti-LDH (LDH) with C60 molecules. The structural characteristics of the resulting products (C60/LDH) were studied using a variety of characterization methods, and the photocatalytic activities of C60/LDH were tested using Orange II (OII) as a model contaminant under simulated solar irradiation. The FT-IR spectra showed that the characteristic mode of C60 at 1182 cm^{-1} split into two peaks at approximately 1240 and 1156 cm^{-1}; in addition, the Raman spectra showed the band at 1422 cm^{-1} for C60 was upshifted to 1431 cm^{-1} with the increased doping amount of C60. In addition, the XPS spectra revealed that the peaks of O1s, Zn 2p, and Ti 2p were downshifted slightly. These results demonstrated that chemical interaction existed between C60 and LDH on C60/LDH. The UV–vis diffuse reflectance spectra confirmed that the absorbance of C60/LDH in visible-light region enhanced markedly, as compared with that of pristine LDH. The photoluminescence (PL) spectroscopic measurement revealed that the C60/LDH composites exhibited much weaker PL intensity than that of LDH sample, and the transient photocurrent (*I–V*) analysis showed that C60/LDH had higher photocurrent density than pristine LDH. The results of PL spectra and *I–V* analysis suggested that C60 molecule could effectively transfer the photoelectrons from the conduction band of LDH, leading to a lower recombination rate of the photo-induced electrons and holes. The photocatalytic experiments showed that C60/LDH had much higher photocatalytic activity in the decolorization of OII than that of pristine LDH, and 2%C60/LDH composite exhibited the highest photocatalytic activity. Furthermore, the stability test indicated that the decolorization efficiency of OII by 2%C60/LDH was still quite efficient after being used for 5 cycles.

1. Introduction

Photocatalysis has received considerable attention for its potential to meeting clean energy demand and solving environmental problems by using solar energy [1–7]. The development of effective semiconductor photocatalysts, therefore, has drawn significant attentions by scientists from various disciplines, such as material science and environmental science.

Layered double hydroxides (LDH) are a class of clays with brucite-like layers and interlayer anions, and they have attracted increasing interests in the field of environmental catalysis [8–10]. Thanks to their tunability of metal compositions and metal ratio, LDH with photocatalytic activities can be easily synthesized by choosing proper metals, which have drawn particular interests [11–13]. Many of the reported LDH photocatalysts showed quite effective degradation activity of organic contaminants [11,14]. Li et al. [9] pointed out that the photoactive elements (e.g., Ti, Cr, Zn) incorporated into LDH matrix could provide great potential in fabricating LDH-based photocatalysts with desired properties [14–19].

* Corresponding authors.
E-mail address: zhurl@gig.ac.cn (R. Zhu).

http://dx.doi.org/10.1016/j.molcata.2016.11.031
1381-1169/

Among the various LDH photocatalysts reported in literatures, Zn/Ti-LDH was shown to have high photocatalytic activity in the degradation of organic contaminants [11,17,20]. However, Li et al. [21] pointed out that the mobility of photon-generated carrier of Zn/Ti-LDH was still not efficient enough. Moreover, Zn/Ti-LDH was mainly activated by UV-light (4% of solar light), resulting in a relatively low photoelectronic transition efficiency. Therefore, further studies are needed to improve the separating efficiency of photo-induced electrons and holes, and enhance the solar light absorption property of Zn/Ti-LDH.

On the other hand, many studies discovered that the addition of functional carbon materials could improve electron-hole separation efficiency and enhance the visible-light response of photocatalysts [21–27]. Recently, C60, one type of functional carbon materials, has drawn much interest in enhancing the photocatalytic activity of the photocatalysts [28–32]. C60 with the delocalized conjugated structures can efficiently arouse a rapid photo-induced charge separation and a lower recombination rate of the photo-induced electrons and holes [28,29]. A number of literatures pointed out that C60 possesses high performance in carrier transmission and broad absorbance in visible light region [30,31,33]. From the perspective of the excellent properties of C60, hybridizing C60 with Zn/Ti-LDH should be beneficial to improving the photocatalytic performance of Zn/Ti-LDH.

In the present work, we explored the role of C60 towards the photochemical performance of the hybridized C60/LDH composites. The structural characteristics of C60/LDH with various C60 content were first studied, and then, their photochemical properties were evaluated by photocatalytic degradation of orange II (OII) under simulated solar irradiation. Based on the characterization and decolorization results, the possible photocatalytic mechanism was proposed. The results of this work demonstrated that hybridizing C60 with Zn/Ti-LDH could improve the separating efficiency of photo-induced electrons and holes, and extend the absorbance from UV light region to visible light region, which then resulted in enhanced photocatalytic activity of C60/LDH composites.

2. Experiment

2.1. Materials

C60 (99%) was obtained from Suzhou Dade Carbon Nanotechnology Co., Ltd. HNO_3 (AR) was provided by Guangzhou Chemical Reagent Factory. $Zn(NO_3)_2{\cdot}6H_2O$ (AR) was purchased from Tianjin Kermel Chemical Reagent Co., Ltd. NaOH (96%), $TiCl_4$ (99%), and urea (99%) were purchased from Tianjin Fu Chen Chemical Reagent Factory Ltd. OII (85%) was obtained from Aladdin Industrial Corporation (Shanghai, China). All reagents were used as received. All labware were cleaned by soaking overnight in diluted HCl solution and washed in ultra-pure water (>18 MΩ/cm) before the experiments.

2.2. Synthesis of Zn/Ti-LDH

The Zn/Ti-LDH (molar ratio of $Zn^{2+}/Ti^{4+} = 2$) was prepared by co-precipitation of zinc and titanium salts from homogeneous solution. A typical synthetic procedure is as follows: 0.22 mL of $TiCl_4$, 1.19 g of $Zn(NO_3)_2{\cdot}6H_2O$, and 3.0 g of urea were dissolved in 100 mL deionized water under vigorous stirring. The resulting reactant was aged in an autoclave at 130 °C for 48 h. The precipitate was centrifuged and washed thoroughly with ultra-pure water. Then, the material was dried at 80 °C overnight, and then ground to pass through a 100-mesh sieve.

2.3. Synthesis of C60/LDH

An appropriate amount of C60 was added into toluene and sonicated for 30 min to thoroughly disperse C60. LDH powder (1 g) was added into the above solution and sonicated for 10 min. The mixture was stirred for 24 h in a dark and sealed place. After that, toluene was removed by heating and evaporating. Then the material was dried at 80 °C for 12 h.

2.4. Characterization

XRD patterns were obtained using a Bruker D8 ADVANCE X-ray diffractometer (Karlsruhe, German). The measurements were operated at 40 kV and 40 mA with Cu Kα radiation, and the 2θ range between 3° and 70° was recorded with a scanning speed of 3°/min.

N_2 adsorption–desorption was carried out at 100 °C on an Autosorb-6b apparatus from Quanta Chrome Instruments. Prior to the analysis, the samples were degassed in a vacuum at 100 °C for 12 h. The specific surface areas were calculated by the Brunauer–Emmett–Teller (BET) method, and the pore size distribution and total pore volume were determined by the density functional theory (DFT) method.

The scanning electron microscopy (SEM) images were recorded by a field emission scanning electron microscopy (Carl Zeiss SUPRA55SAPPHIR) with energy dispersive X-ray spectroscopy (EDX) for the determination of metal composition.

FT-IR characterization was carried out on a Brucker Vertex-70 FT-IR spectrophotometer. The spectra over the range of 4000–400 cm^{-1} were recorded with a resolution of 1.0 cm^{-1}.

Raman spectra were acquired using a Renishaw RM 2000 spectrometer equipped with a CCD detector (1100 × 330 pixels) and a 200 mW Ar-ion laser to probe samples in the micro-Raman system with single grating 0.5 m spectrometer. The 532 nm laser wavelength was used for Raman scattering with a spectral range of 100–4000 cm^{-1}.

X-ray photoelectron spectroscopy (XPS) analyses were carried out by a Thermo Fisher Scientific K-Alpha spectrometer. The C1s peak from the adventitious carbon-based contaminant with bind energy of 284.8 eV was used as the reference for calibration.

The UV–vis diffuse reflectance spectra were measured by Shimadzu UV-2550 double-beam digital spectrophotometer equipped with conventional components of a reflectance spectrometer, and $BaSO_4$ was used as reference.

Photoluminescence (PL) spectra were measured at room temperature on a Fluorescence Spectrophotometer (F-7000, Hitachi, Japan) with an excitation wavelength of 365 nm. The scanning speed was 1200 nm/min and the PMT voltage was 700 V. The widths of the excitation slit and emission slit were both 5.0 nm.

The photoelectrochemical measurements were performed with a CHI 760D electrochemical workstation (CH Instruments, Inc.) using a three-electrode system at room temperature. The electrolyte was 0.5 mol/L Na_2SO_4 solution, and a 500 W Xe lamp was used as the light source.

2.5. Photocatalytic experiments

The photocatalytic activity of the obtained materials was monitored by the degradation of OII under simulated solar light irradiation using a 1000 W xenon lamp (100–105 mW/cm^2). The experiments were conducted in a photochemical reaction instrument (BL-GHX-V, Shanghai Depai Biotech. Co. Ltd., China). Typically, a mixture of 50 mL OII (100 mg/L) solution and 50 mg catalyst was vigorously stirred for 2 h. The initial pH value of the solution (pH = 7) was adjusted by adding 0.1 mol/L NaOH and HNO_3. During the photolysis process, samples were collected at desired intervals from the solution, which was followed by centrifugation

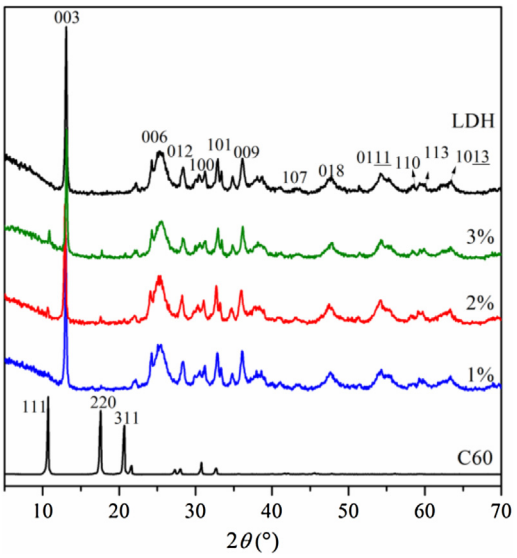

Fig. 1. XRD patterns of C60/LDH samples with various C60 contents.

to separate the solid from the liquid before measurement. The filtrates were tested by measuring the absorbance at 485 nm using UV–vis spectrophotometer (759S, Shanghai JingHua Instrument Co. Ltd., China), and the blank reaction was also carried out by the same procedure without adding any catalysts.

2.6. Photocatalytic stability experiments

2%C60/LDH was used repeatedly for degrading OII to evaluate its photocatalytic stability. The experimental process was similar to the above photocatalytic experiments. After reaction in each run, the photocatalyst was collected by centrifugation for the next use.

3. Results and discussion

3.1. Structural characterization results

The XRD patterns of Zn/Ti-LDH and C60/LDH were collected (Fig. 1). The XRD pattern of LDH showed both sharp and symmetrical reflection at 13.1°, which, together with the reflections of (006), (009), (100), (101), (012), (110), and (113), could be indexed to typical LDH [20,34]. After being modified with C60, the XRD patterns had no obvious changes, indicating the combination of C60 with LDH could not evidently alter the crystal structure of the host.

The morphologies of the as-prepared pristine LDH and 2%C60/LDH were shown (Fig. 2a–d). The high-resolution SEM image of LDH (Fig. 2a) clearly exhibited the presence of hierarchical structure consisting of two-dimensional thin nanoflakes, which was typical for the LDH morphology [20,34]. The EDS Mapping was selected for further analysis of elemental distribution on the LDH sample (Fig. 2b-b_3). The elemental mapping images displayed the uniform and homogeneous distribution of O, Zn, and Ti. Different from the pristine LDH material with aggregation (Fig. 2c), 2%C60/LDH (Fig. 2d) were highly dispersed and had smaller average size.

The nitrogen adsorption–desorption isotherms of LDH and 2%C60/LDH samples were compared (Fig. 3). The two samples exhibited a typical IVa isotherm with a H3-type hysteresis loop ($P/P_0 > 0.4$) [35], indicating the presence of mesopores with slit-shape on these samples [36]. Furthermore, the result could be confirmed by the corresponding wide distribution of pore size (inset in Fig. 2). The pore width of LDH was about 4.97 nm, while that of 2%C60/LDH was about 4.75 nm. The slight decrease of pore width might be ascribed to the occupation of the card-house-like structure of the LDH nanoplates by C60, similar to the result of C60 modified g-C_3N_4 [30]. After the hybridization of C60, both the BET surface area and pore volume of the resulting materials were slightly decreased (Table 1), probably due to the pore occupation by C60. Analogously, Zhang et al. [37] found that after immobilization

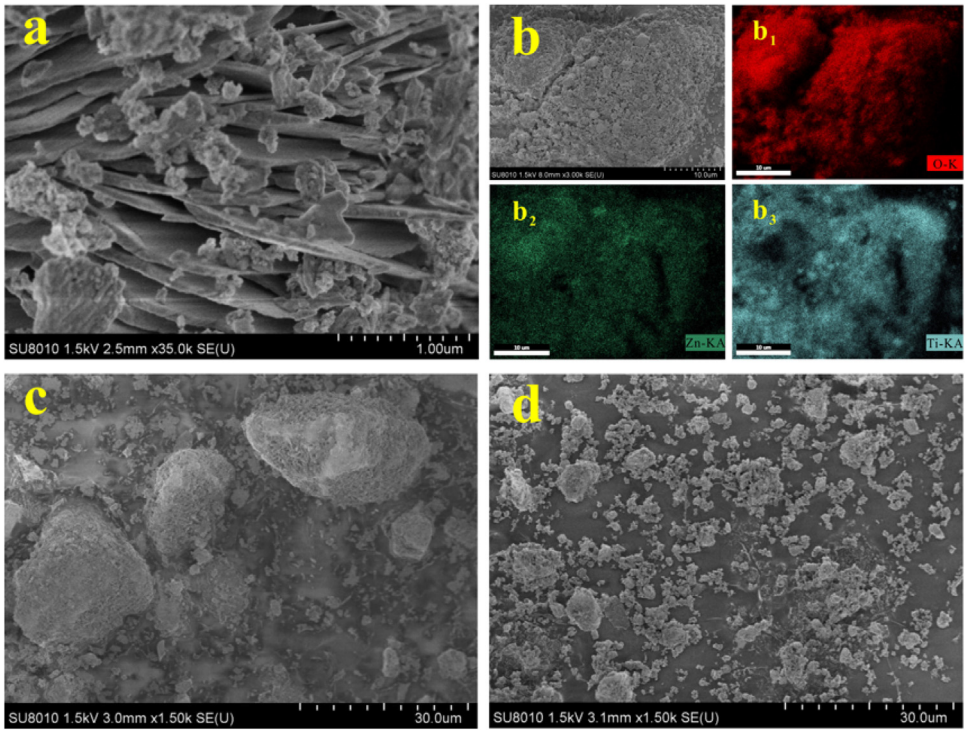

Fig. 2. (a) High-resolution SEM image of pristine LDH. (b) SEM image for LDH sample; (b_1)-(b_3) EDS mapping images of the O, Zn, Ti elements respectively. Low-resolution SEM image of (c) LDH and (d) 2%C60/LDH.

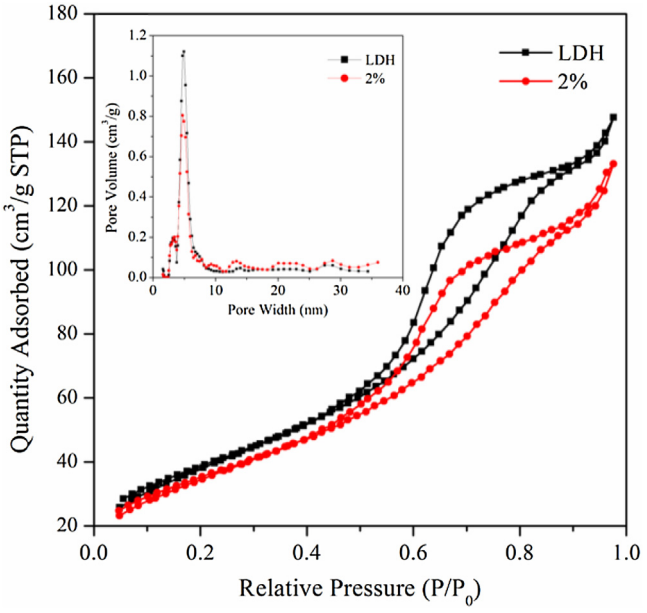

Fig. 3. N_2 adsorption–desorption isotherms and pore size distribution plots of LDH and 2%C60/LDH samples.

Table 1
The textural properties of C60/LDH samples with various C60 contents.

Samples	Surface area (m^2/g)	Pore volume (cm^3/g)	Pore size (nm)
LDH	141.3	0.210	4.97
1%	135.8	0.199	4.75
2%	129.3	0.191	4.75
3%	128.6	0.193	4.75

of Rh–MonoPhos on porous silicas, the BET surface area and pore volume decrease obviously, probably due to the pore occupation by Rh–MonoPhos.

To have an insight into the nature of the interfacial interaction between C60 and LDH on the C60/LDH composites, FT-IR and Raman spectra were collected in this work (Fig. 4). In the FT-IR spectra range of 1800–1000 cm^{-1} (Fig. 4a), the band at 1638 cm^{-1} for LDH could be assigned to water bending vibration [38], and the bands at 1510 and 1385 cm^{-1} can be assigned to the vibration of interlayer NO_3^- [34,39]. The peaks at 1182 and 1428 cm^{-1} on C60 could be attributed to the internal modes of the C60 molecule [40]. With the loading of C60 on LDH, the characteristic mode at 1182 cm^{-1} of C60, which was very sensitive to charge transfer, split into two peaks at approximately 1240 and 1156 cm^{-1}, similar to the result of C60 hybridized with other semiconductors [28,32]. For example, Zhang et al. [32] found that the characteristic mode at 1182 cm^{-1} of C60 on C60-hybridized TiO_2 composites split into two peaks at about 1225 and 1159 cm^{-1}, and they proposed the occurrence of charge-transfers from TiO_2 to C60 by the chemical interaction between C60 and TiO_2 on C60-hybridized TiO_2. Accordingly, we suggested that the chemical interaction existed between LDH and C60 on C60/LDH.

The interaction between C60 and LDH could also be revealed by Raman spectral characterization (Fig. 4b). The Raman spectrum of pristine C60 showed bands at 1422, 1464, and 1569 cm^{-1}, which were assigned to the vibration frequencies of Hg(7), Ag(2), and Hg(8) modes, respectively [41]. Some changes occurred in the Raman spectrum after C60 being hybridized with LDH. The band at 1422 cm^{-1} was upshifted with increasing amount of C60. The largest upshift of this band was approximately 9 cm^{-1} in the case of 3%C60/LDH. In addition, the Ag(2) symmetry band at 1464 cm^{-1}, which was related to the carrier transfer [28], was slightly downshifted and broadened with increasing C60 amount. As such, both the FT-IR and Raman spectral characterization results demonstrated that chemical interaction existed between C60 and LDH on C60/LDH.

XPS is a surface-specific characterization tool, which can be used to determine the chemical environment and elemental oxidation state [42]. To find more evidences about the chemical interaction between C60 and LDH of C60/LDH, XPS spectra of C60/LDH samples with various C60 contents were collected (Fig. 5). The C 1s peaks of the C60/LDH samples showed no significant changes compared with that of pure LDH. The peaks with binding energies of 530.0 and 532.3 eV could be assigned to the O 1s peaks, which corresponded to the "O^{2-}" ions of the crystalline network of Zn/Ti-LDH and the adsorbed oxygen, respectively [43]. With the loading of C60 on LDH, the O 1s peaks were downshifted, indicating a lower electron density [43]. In addition, the peaks of Zn 2p and Ti 2p were also downshifted slightly. It may be attributed to the formation of covalent bond (Zn—O≡C60, Ti—O≡C60) between C60 and the surface groups of LDH (≡Zn—OH, ≡Ti—OH). This assumption was original from the similar research of fullerol–titania charge-transfer-mediated photocatalysis. Park et al. [44] deduced that fullerols on TiO_2 may form surface complexes through covalent bond formation between the surface titanol group (≡Ti—OH) and fullerol. Therefore, the XPS spectra results further confirmed that chemical interaction existed between C60 and LDH on C60/LDH.

The UV–vis diffuse reflectance spectrum of LDH sample showed an absorption edge around 450 nm (Fig. 6). On the other hand, a wide absorption ranged from 200 to 750 nm was observed for all of the C60/LDH samples. Moreover, the absorption intensity increased evidently with the addition of 1% C60, but the increment was insignificant with the further increase of C60 content (i.e., from 1% to 2% and 3%). Probably because C60 aggregated to form cluster on the surface of C60/LDH at high C60 content [28].

3.2. Photo-decolorization of OII

To examine the photocatalytic activities of the as-prepared photocatalysts, several photocatalytic experiments using LDH and C60/LDH were carried out for OII decolorization in dark (Fig. 7a) and under simulated solar irradiation (Fig. 7b). In the case of C60/LDH samples with various C60 contents, only about 10% OII could be decolorized in dark, indicating poor adsorption efficiency of OII on the as-prepared photocatalysts.

For photocatalytic experiments under the irradiation of simulated solar, the results showed that only 73% and 47% OII could be decolorized by pristine LDH and pure C60 in 120 min, respectively, while the decolorization rate by C60/LDH samples was all above 92%. The decolorization rate of photocatalytic reaction was influenced by the content of C60. In particular, the decolorization efficiency of OII first increased with rising C60 content from 0 to 2%, and then begun to decrease when the content of C60 was larger than 2%. Among the series of as-prepared photocatalysts, 2%C60/LDH sample exhibited the highest activity with an OII decolorization rate of 96%.

These decolorized processes were fittied to pseudo-first-order kinetics (with the obtained linearly dependent coefficients all over 0.95) (Fig. 8), in which the value of rate constant (K_{app}) is equal to the corresponding slope of the fitting line. The K_{app} of 2%C60/LDH was 0.0237 min^{-1}, which was about 2.5 times as high as that of pristine LDH. This result implied that the interaction between C60 and LDH photocatalysts took an important role in the enhancement of photoactivity [28,29].

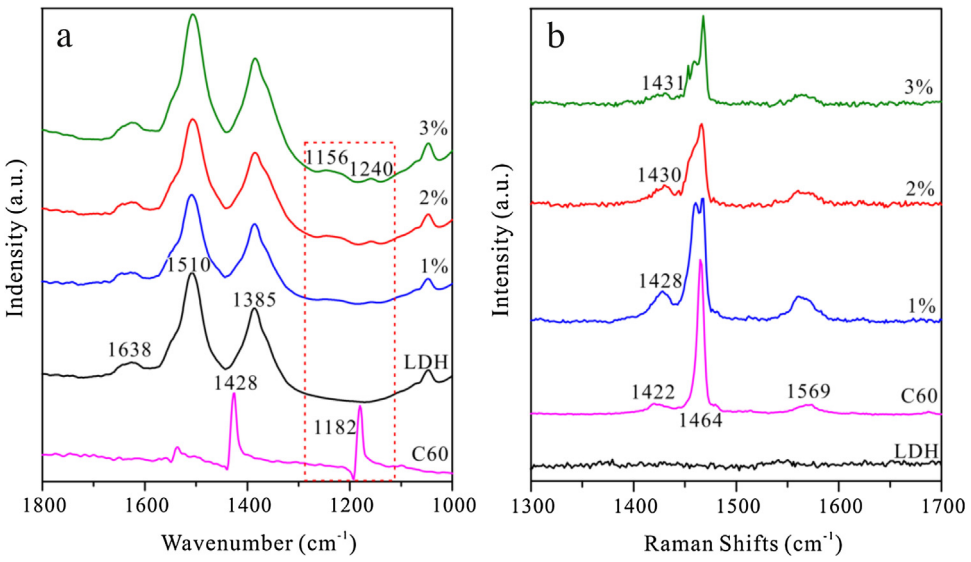

Fig. 4. (a) FT-IR patterns and (b) Raman patterns of C60/LDH samples with various C60 contents.

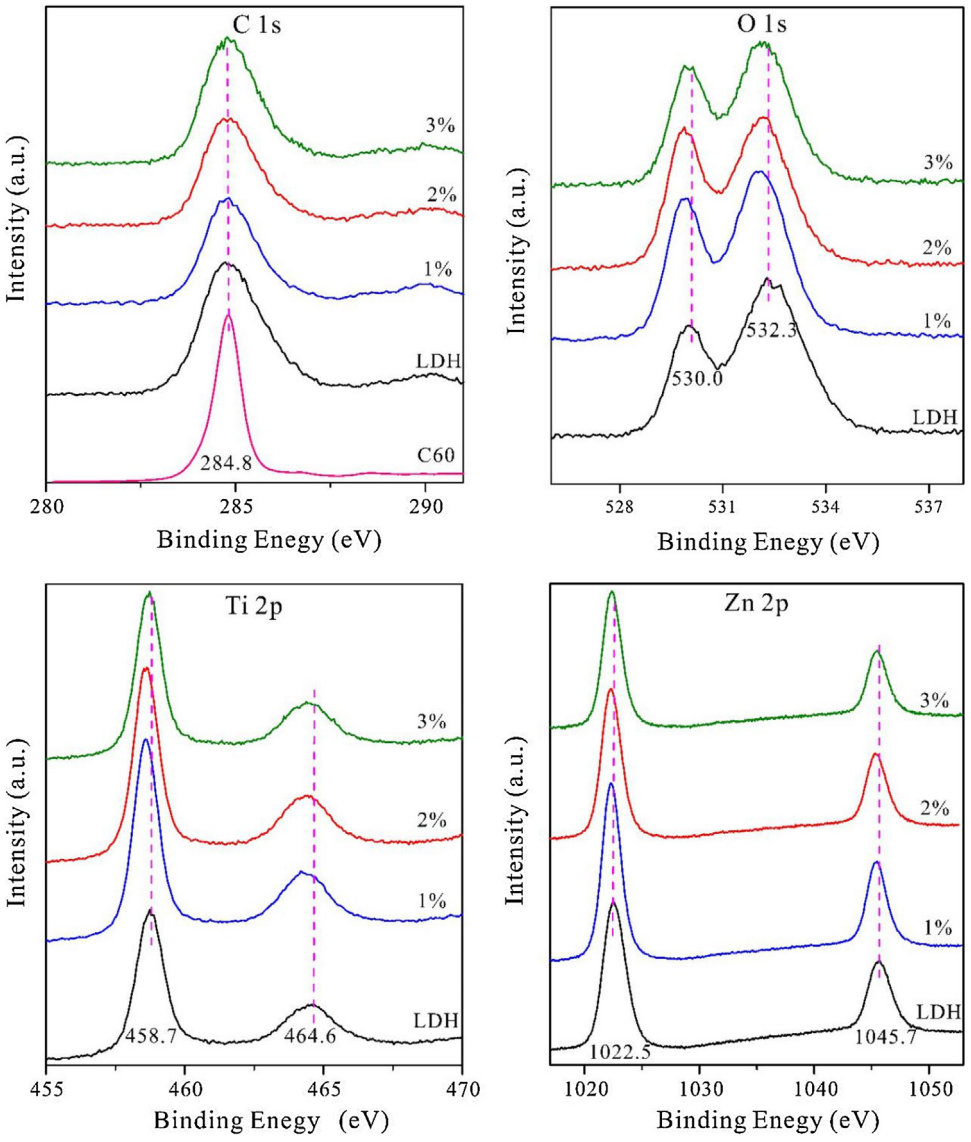

Fig. 5. XPS spectra of C60/LDH samples with various C60 contents.

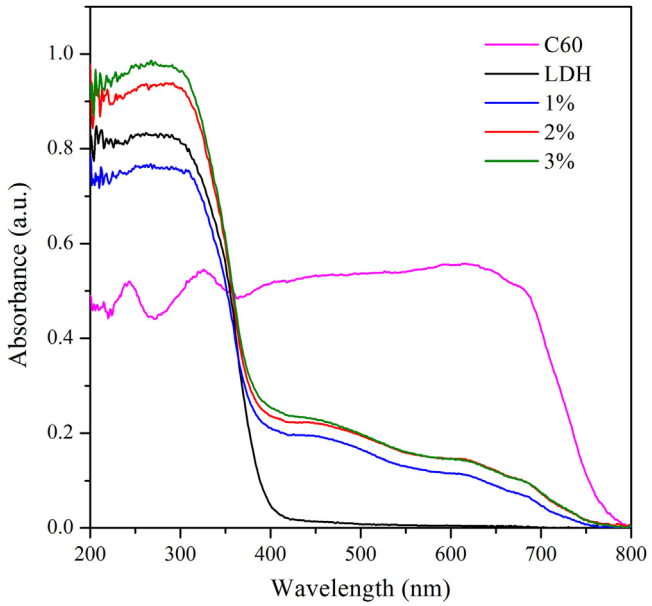

Fig. 6. UV–vis diffuse reflectance spectra of C60/LDH samples with various C60 contents.

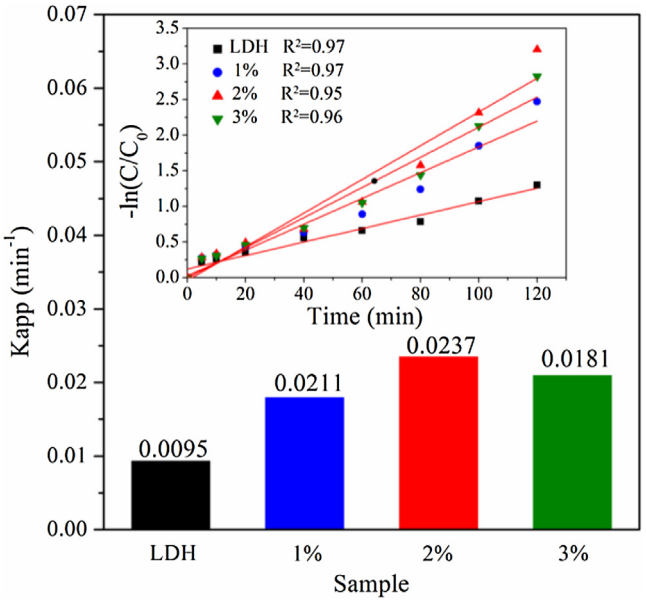

Fig. 8. Apparent rate constants for the photocatalytic degradation of OII by C60/LDH samples with various C60 contents. Inset: Pseudo-first order kinetics for the photocatalytic degradation of OII on C60/LDH samples with various C60 contents.

3.3. Stability test of photocatalysts

To evaluate the photochemical stability of the catalyst, the repeated experiments for the photocatalytic decomposition of OII under the same conditions over as-prepared 2%C60/LDH composite were conducted (Fig. 9). The obtained results revealed that the decolorization efficiency of OII (>85%) was still quite efficient after being used for 5 cycles. The decolorization efficiency of OII slightly decreased in the first three cycles, but the decrement was insignificant in the following cycles, indicating good stability of 2%C60/LDH. The slight decrease of the photocatalytic performance might be attributed to the loss of the photocatalysts during the recovery process of the photocatalyst via centrifugation.

3.4. PL spectra and I–V analysis

Photoluminescence (PL) spectroscopic measurement and transient photocurrent (*I–V*) analysis have often been used to reveal the efficiency of charge carrier trapping, transfer, and separation, and to investigate the fate of photogenerated electrons and holes in semiconductors [45–47]. The PL emission spectra of the samples were collected in the wavelength range of 400–600 nm (Fig. 10a), which showed that C60/LDH composites had much weaker PL intensity than LDH. It implied that the hybridized C60 could greatly influence PL intensity. Further, the PL intensity of C60/LDH decreased with increasing C60 loading and then reached a minimum at a C60 loading of 2%. However, the PL intensity increased when C60 loading further rose to 3%. This might be attributed to the factor that the redundant C60 became the radiative recombination center of photo-induced electron-hole pairs [48]. Moreover, 2%C60/LDH sample showed the lowest PL intensity, which was consistent with its highest photocatalytic activity (Fig. 7). Nayak et al. [25]. showed the similar result in the photocatalytic activity towards water oxidation and reduction reaction of g-C_3N_4/NiFe-LDH composite photocatalyst. In addition, the transient photocurrent responses (Fig. 10b) showed that C60/LDH exhibited higher photocurrent density compared with pristine LDH. It was clearly showed that the 2%C60/LDH electrode was almost three times higher than that of the pure LDH, which indicated more efficient photo-induced charge separation and faster charge transfer in C60/LDH samples. These facts suggested that the hybridized C60 molecule could effec-

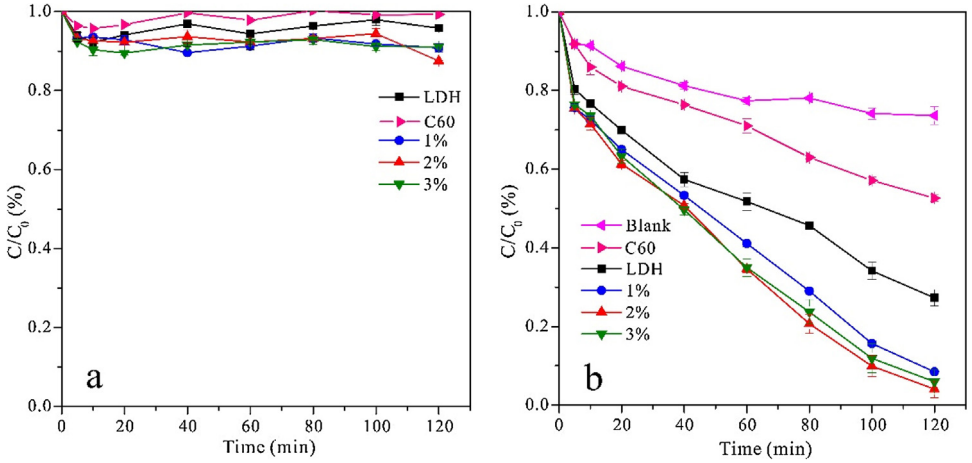

Fig. 7. Decolorization kinetics of OII on C60/LDH samples (a) in dark and (b) under solar irradiation.

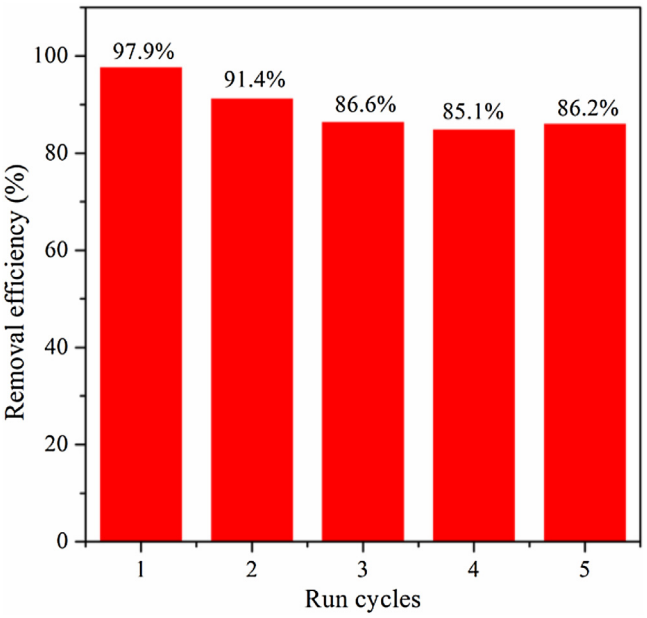

Fig. 9. Stability test of 2%C60/LDH.

tively transfer the photoelectrons from conduction band of LDH, inhibiting a direct recombination of electrons and holes. Thus, more electrons and holes could participate in the photocatalytic reaction, contributing to higher photocatalytic activity.

3.5. Photocatalytic mechanism

Based on the above results, a mechanism for separation and transportation of electron–hole pairs at the interface of C60/LDH was proposed (Scheme 1). Under the irradiation of simulated solar, electrons were excited from the valence band to the conduction band of LDH. Normally, these charge carriers would quickly recombine and only a fraction of electrons could participate in the photocatalytic reaction. However, the level of conduction band in Zn/Ti-LDH (−0.56 eV vs NHE) was lower than the reduction potential of C60 (−0.2 eV vs NHE) [49,50]. Therefore, the photogenerated electron can easily emigrate from the conduction band of LDH to C60 molecules with the interaction between LDH and C60, inhibiting a direct recombination of electrons and holes. The transferred electrons would accumulate on the C60 nanoparticles to capture the adsorbed O_2 on LDH surface to form superoxide radical ($O_2^{\bullet -}$), which then participated in photocatalytic oxidation reaction. Meanwhile, on the valence band of LDH, the high separation efficiency of photo-induced electron–hole pairs resulted in the increase of holes. The holes can react with water to produce

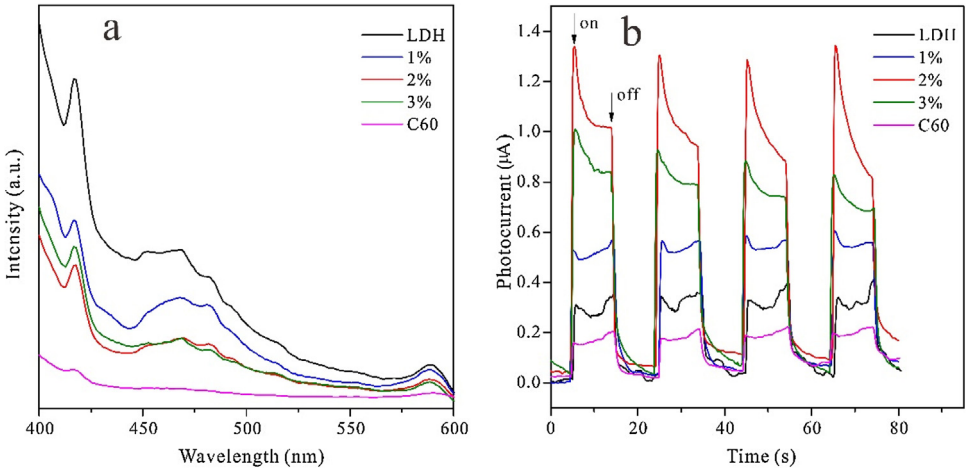

Fig. 10. (a) Photoluminescence spectra and (b) transient photocurrent of C60/LDH samples with various C60 contents.

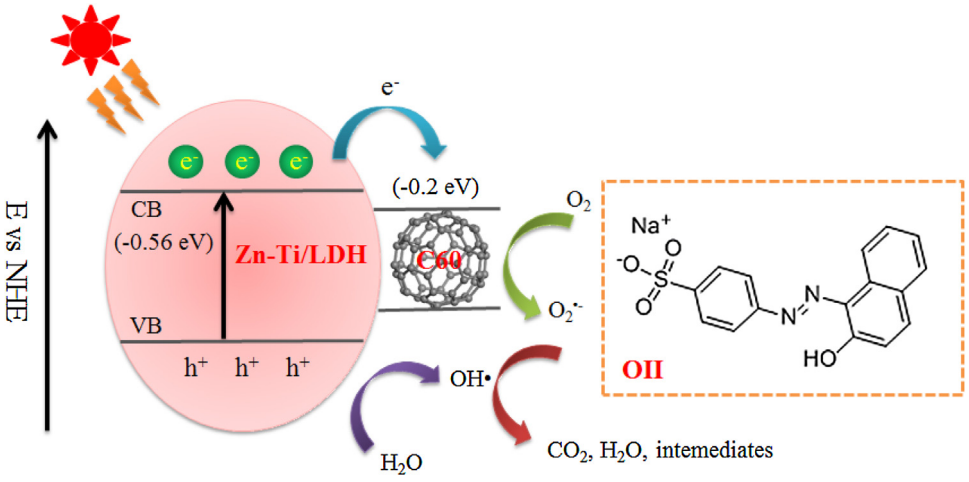

Scheme 1. Possible photocatalytic mechanism.

hydroxyl radical ($OH^{\bullet}$), which is a strong oxidizing reagent for the degradation of OII.

4. Conclusion

In this work, C60/LDH composites with high photocatalytic activity were synthesized successfully by hybridizing LDH with C60. C60 molecules were dispersed on the surface of the LDH samples and strong chemical interactions were formed between them. The C60/LDH composites had higher photocatalytic activity in the decolorization of OII than that of pristine LDH, and 2%C60/LDH composite exhibited the highest photocatalytic activity. The evident enhancement of photocatalytic performance could be attributed to the rapid electron transition and charge separation efficiency by C60 on C60/LDH composites, as well as the extended absorption range from UV to visible region.

Acknowledgments

This work was financially supported by the National Natural Science Foundation of China (41572031, 41322014, 21177104), National Youth Top-notch Talent Support Program, Guangdong Provincial Youth Top-notch Talent Support Program (2014TQ01Z249), and CAS/SAFEA International Partnership Program for Creative Research Teams (20140491534).

References

[1] A. Fujishima, Nature 238 (1972) 37–38.
[2] Z. Zhang, C.-C. Wang, R. Zakaria, J.Y. Ying, J. Phys. Chem. B 102 (1998) 10871–10878.
[3] M. Anpo, M. Takeuchi, J. Catal. 216 (2003) 505–516.
[4] T. Ohno, M. Akiyoshi, T. Umebayashi, K. Asai, T. Mitsui, M. Matsumura, Appl. Catal. A: Gen. 265 (2004) 115–121.
[5] H. Kato, K. Asakura, A. Kudo, J. Am. Chem. Soc. 125 (2003) 3082–3089.
[6] R.I. Bickley, T. Gonzalez-Carreno, J.S. Lees, L. Palmisano, R.J. Tilley, J. Solid State Chem. 92 (1991) 178–190.
[7] S. Martha, A. Nashim, K.M. Parida, J. Mater. Chem. A 1 (2013) 7816.
[8] S. He, Z. An, M. Wei, D.G. Evans, X. Duan, Chem. Commun. 49 (2013) 5912–5920.
[9] C. Li, M. Wei, D.G. Evans, X. Duan, Small 10 (2014) 4469–4486.
[10] L. Mohapatra, K. Parida, J. Mater. Chem. A 4 (2016) 10744–10766.
[11] S.J. Xia, F.X. Liu, Z.M. Ni, J.L. Xue, P.P. Qian, J. Colloid Interface Sci. 405 (2013) 195–200.
[12] N. Baliarsingh, K.M. Parida, G.C. Pradhan, Ind. Eng. Chem. Res. 53 (2014) 3834–3841.
[13] M. Laipan, R. Zhu, J. Zhu, H. He, J. Mol. Catal. A: Chem. 415 (2016) 9–16.
[14] L. Mohapatra, K. Parida, Sep. Purif. Technol. 91 (2012) 73–80.
[15] M. Shao, J. Han, M. Wei, D.G. Evans, X. Duan, Chem. Eng. J. 168 (2011) 519–524.
[16] K.-i. Katsumata, K. Sakai, K. Ikeda, G. Carja, N. Matsushita, K. Okada, Mater. Lett. 107 (2013) 138–140.
[17] S.-J. Xia, F.-X. Liu, Z.-M. Ni, W. Shi, J.-L. Xue, P.-P. Qian, Appl. Catal. B—Environ. 144 (2014) 570–579.
[18] N. Baliarsingh, L. Mohapatra, K. Parida, J. Mater. Chem. A 1 (2013) 4236.
[19] L. Mohapatra, K. Parida, M. Satpathy, J. Phys. Chem. C 116 (2012) 13063–13070.
[20] M.F. Shao, J.B. Han, M. Wei, D.G. Evans, X. Duan, Chem. Eng. J. 168 (2011) 519–524.
[21] B. Li, Y. Zhao, S. Zhang, W. Gao, M. Wei, ACS Appl. Mater. Interfaces 5 (2013) 10233–10239.
[22] M. Lan, G. Fan, L. Yang, F. Li, RSC Adv. 5 (2015) 5725–5734.
[23] Y. Cao, G.T. Li, X.B. Li, Chem. Eng. J. 292 (2016) 207–223.
[24] M. Daud, M.S. Kamal, F. Shehzad, M.A. Al-Harthi, Carbon 104 (2016) 241–252.
[25] S. Nayak, L. Mohapatra, K. Parida, J. Mater. Chem. A 3 (2015) 18622–18635.
[26] S. Pany, K.M. Parida, Phys. Chem. Chem. Phys. 17 (2015) 8070–8077.
[27] S. Patnaik, S. Martha, S. Acharya, K.M. Parida, Inorg. Chem. Front. 3 (2016) 336–347.
[28] H. Fu, T. Xu, S. Zhu, Y. Zhu, Environ. Sci. Technol. 42 (2008) 8064–8069.
[29] S. Zhu, T. Xu, H. Fu, J. Zhao, Y. Zhu, Environ. Sci. Technol. 41 (2007) 6234–6239.
[30] X.J. Bai, L. Wang, Y.J. Wang, W.Q. Yao, Y.F. Zhu, Appl. Catal. B—Environ. 152 (2014) 262–270.
[31] G. Li, B. Jiang, X. Li, Z. Lian, S. Xiao, J. Zhu, D. Zhang, H. Li, ACS Appl. Mater. Interfaces 5 (2013) 7190–7197.
[32] L. Zhang, Y. Wang, T. Xu, S. Zhu, Y. Zhu, J. Mol. Catal. A: Chem. 331 (2010) 7–14.
[33] X. Zhao, H. Liu, Y. Shen, J. Qu, Appl. Catal. B: Environ. 106 (2011) 63–68.
[34] O. Saber, H. Tagaya, J. Inclusion Phenom. Macrocyclic Chem. 45 (2003) 107–115.
[35] M. Thommes, K. Kaneko, A.V. Neimark, J.P. Olivier, F. Rodriguez-Reinoso, J. Rouquerol, K.S.W. Sing, Pure Appl. Chem. 87 (2015).
[36] J.L. Gunjakar, T.W. Kim, H.N. Kim, I.Y. Kim, S.J. Hwang, J. Am. Chem. Soc. 133 (2011) 14998–15007.
[37] X. Zhang, X. Liu, J. Peng, Y. Zhao, Q. Yang, Catal. Sci. Technol. 4 (2014) 1012.
[38] F. Cavani, F. Trifirò, A. Vaccari, Catal. Today 11 (1991) 173–301.
[39] S.-J. Xia, F.-X. Liu, Z.-M. Ni, W. Shi, J.-L. Xue, P.-P. Qian, Appl. Catal. B: Environ. 144 (2014) 570–579.
[40] S.G. Stepanian, V.A. Karachevtsev, A.M. Plokhotnichenko, L. Adamowicz, A.M. Rao, J. Phys. Chem. B 110 (2006) 15769–15775.
[41] D.S. Bethune, G. Meijer, W.C. Tang, H.J. Rosen, W.G. Golden, H. Seki, C.A. Brown, M.S. de Vries, Chem. Phys. Lett. 179 (1991) 181–186.
[42] S. Samanta, S. Martha, K. Parida, ChemCatChem (2014) 1453–1462.
[43] J.-C. Dupin, D. Gonbeau, P. Vinatier, A. Levasseur, Phys. Chem. Chem. Phys. 2 (2000) 1319–1324.
[44] Y. Park, N.J. Singh, K.S. Kim, T. Tachikawa, T. Majima, W. Choi, Chemistry 15 (2009) 10843–10850.
[45] G. Zhu, W. Que, J. Zhang, Alloys Compd. 509 (2011) 9479–9486.
[46] J. Yu, Z. Wu, C. Gong, W. Xiao, L. Sun, C. Lin, Nanomaterials 6 (2016) 107.
[47] S. Patnaik, S. Martha, K.M. Parida, RSC Adv. 6 (2016) 46929–46951.
[48] T. Xu, R. Zhu, J. Zhu, X. Liang, G. Zhu, Y. Liu, Y. Xu, H. He, RSC Adv. 6 (2016) 85962–85969.
[49] G. Chen, S. Qian, X. Tu, X. Wei, J. Zou, L. Leng, S. Luo, Appl. Surf. Sci. 293 (2014) 345–351.
[50] P.V. Kamat, I. Bedja, S. Hotchandani, J. Phys. Chem. 98 (1994) 9137–9142.